J Nanostruct 16(1): 484-493, Winter 2026

RESEARCH PAPER

Co-precipitation Synthesis of $Mg_{0.2}Cu_{0.3}Zn_{0.5}Fe_2O_4$ Nanoparticles: Study Their Magnetic and Visible-light Photocatalytic Properties

Mustafa Saade Shakir [1]*, *Ban Samary Atyah* [2]

[1] *Market Research and Consumer Protection Center, University of Baghdad, Iraq*

[2] *Environmental Research Center, University of Technology, Iraq*

ARTICLE INFO

Article History:
Received 06 September 2025
Accepted 20 December 2025
Published 01 January 2026

Keywords:
Co-precipitation
Magnetic properties
$Mg_{0.2}Cu_{0.3}Zn_{0.5}Fe_2O_4$ nanoparticles
Photocatalyst activity
Visible light

ABSTRACT

$Mg_{0.2}Cu_{0.3}Zn_{0.5}Fe_2O_4$ (MCZFO) nanoparticles were synthesized through co-precipitation reaction in the presence of Tween 20 and polyethylene glycol (PEG) as capping agents. The use of different capping agents resulted in nanoparticles with distinct morphologies, as confirmed by scanning electron microscopy (SEM). Magnetization of the nanoparticles was studied using vibrating sample magnetometer (VSM) analysis, which revealed the ferromagnetic behavior for the nanoparticles. The flake-like nanoparticles synthesized with tween 20 exhibited the higher coercivity value compared to that of synthesized by PEG. Both the synthesized nanoparticles possessed the strong absorption in the visible light region, which was particularly pronounced for the high light-contact surface nanoparticles synthesized using tween 20. Photocatalytic activity of the nanoparticles was assessed for degradation of acid red 88 (AR88) under 120 min visible light illumination. Also, photocatalysis of AR88 was investigated under different experimental conditions, including various amount of the loaded nanoparticles, different pH of AR88 solution, and use of $Na_2S_2O_8$ and H_2O_2 solutions as oxidant agents. The MCZFO nanoparticles exhibited the excellent reusability at 6 successive reaction cycles.

How to cite this article
Shakir M., Atyah B. Co-precipitation Synthesis of $Mg_{0.2}Cu_{0.3}Zn_{0.5}Fe_2O_4$ Nanoparticles: Study Their Magnetic and Visible-light Photocatalytic Properties. J Nanostruct, 2026; 16(1):484-493. DOI: 10.22052/JNS.2026.01.044

INTRODUCTION

The high surface-to-volume ratio endows nanoscale materials with properties distinct from those of their bulk counterparts [1-3]. Because of higher aspect ratio, a significant fraction of atoms are located on the surface of nanomaterials, which modifies the electronic band structure and also increases the number of active sites. As a result, nanomaterials exhibit excellent catalytic, optical, magnetic, and thermal properties that are not observed in bulk materials [4-6]. Utilizing of nanomaterials in many technical area has opened up the doors to address complicated industrial, environmental problems as well as global public health challenges [7-9].

Thanks to appreciable characteristics of nanomaterials, nano-photocatalyst has now inspired researchers to come up an efficient method to solve environmental crisis worldwide [10-12]. Photocatalysis is defined as a specific reaction induced by photo-sensitized catalyst. Titanium dioxide (TiO_2)—a common photocatalyst—is

* *Corresponding Author Email: mustafaaldori85@gmail.com*

activated by absorption of UV light to generate highly reactive radicals, which oxidize organic pollutants in water media [13]. Despite noticeable advantages, common photocatalysts have some limitations, thereby developing new and more efficient photocatalyst is of great interest [14, 15].

Pure TiO_2 suffers from poor sensitization in the visible light region and fast recombination rate of electrons and holes, which reduce its performance for the practical environmental applications [16, 17]. Recently, numerous photocatalysts have been reported in literature. Combination of two or more photocatalyst materials is the great approach to effectively employ the photocatalysis for removing contaminants. For example, real petrochemical wastewater has been treated using Fe and B co-doped TiO_2/carbon nanotubes/WO_3 nanocomposite under natural sunlight irradiation [18]. You et al. reported degradation of antibiotics using plasmonic effect of $Ag/Ag_2O/C_3N_4$ [19]. Also, photocatalytic efficiency of $Mn_{0.5}Cd_{0.5}S/In_2S_3$ has been studied for degradation of antibiotic [20].

Herein, co-precipitation reaction was used to synthesize $Mg_{0.2}Cu_{0.3}Zn_{0.5}Fe_2O_4$ (MCZFO) nanoparticles as the efficient visible-light photocatalyst. Co-precipitation method is known for its versatility, simplicity, and cost-effectiveness [21]. Using proper capping agents is urgent for synthesizing nanoparticles through the co-precipitation method. In this work, tween 20 and polyethylene glycol (PEG 600) to controlling size of the MCZFO nanoparticles.

The magnetic properties of the synthesized MCZFO nanoparticles in the presence of the different capping agents were investigated using vibrating sample magnetometer (VSM) analysis. In addition, photocatalytic efficiency of the MCZFO nanoparticles was assessed for degradation of acid red 88 (AR88) under visible light irradiation. The photocatalytic experiments were conducted in varied conditions to find optimal photoactivity of the MCZFO nanoparticles. To this end, different oxidant agents ($Na_2S_2O_8$ and H_2O_2.) were used. Additionally, the effects of various pH values of the AR88 solution and different amount of loaded MCZFO nanoparticles were studied.

MATERIALS AND METHODS

Co-precipitation synthesis of $Mg_{0.2}Cu_{0.3}Zn_{0.5}Fe_2O_4$ (MCZFO) nanoparticles

The synthetic route of MCZFO nanoparticles is as follows: First, different capping agents were separately dissolved in 50 mL of distilled water. For this purpose, tween 20 and polyethylene glycol (PEG-600) were used. Then, 0.2 mmol of $Mg(NO_3)_2.6H_2O$, 0.3 mmol of $Cu(NO_3)_2.3H_2O$, 0.5 mmol of $Zn(NO_3)_2.6H_2O$, and 2.0 mmol of $Fe(NO_{3)3}.9H_2O$ were added to the above solution and vigorously stirred for 1 h. The pH of solution was adjusted to 9 by adding NaOH solution (0.1 M) dropwise. The solution was then further stirred for more than 2 h. Next, the solid was recovered by centrifugation at 7000 rpm for 15 min. The collected solid was washed several times using ethanol/distilled water solution and then dried in an oven at 100 °C overnight. Finally, the dried solid was heated at 600 °C for 4 h to form pure and crystalline MCZFO nanoparticles. The MCZFO nanoparticles synthesized in the presence of PEG-600 and tween 20 were designated as MCZFO-PEG600 and MCZFO-T20, respectively.

Photocatalytic and magnetic investigations

The photocatalytic activity of both the synthesized MCZFO-PEG600 and MCZFO-T20 were assessed to degradation of acid red 88 (AR88) under visible light irradiation. An aqueous solution of AR88 (50 ppm) was used in the presence of the different loaded of the nanoparticles (0.03, 0.05, and 0.07g). An ordinary halogen lamp (100 W) was used as the visible light source. The container of the dye solution was illuminated from the constant distance of 30 cm. To reach the adsorption/desorption equilibrium between the dye molecules and the nanoparticles, the dye solution containing the nanoparticles were continuously stirred for 20 min in darkness. The degradation level of AR88 was tested at 20 min intervals using a UV/Vis spectrophotometer at maximum absorption wavelength of AR88 (506 nm). The effects of different pH of dye solution and different concentrations of $Na_2S_2O_8$ and H_2O_2 (as oxidant agent) were investigated on the photocatalytic efficiency of the synthesized nanoparticles.

To study the magnetic behavior of the MCZFO-T20 and MCZFO-PEG600, as well as the influence of different capping agents on their magnetization, vibrating sample magnetometer analysis was carried out at the room temperature.

Characterization

Crystal structure of the synthesized nanoparticles was studied using X-ray diffraction

(XRD) pattern by X'pert Pro MPD Philphs (Cu Kα). Morphology and other surface properties of the MCZFO-T20 and MCZFO-PEG600 were studied using field emission scanning electron microcopy (FESEM) by TESCAN Mira3 equipped with proper detector to record the energy dispersive X-ray (EDX) spectrum for compositional analysis of the nanoparticles. Vibrating sample magnetometer (VSM) analysis (VSM MDKB) was used to investigate magnetic properties of the synthesized MCZFO-T20 and MCZFO-PEG600 nanoparticles. UV/Vis absorption spectra of the nanoparticles were recorded by JASCO UV/Vis/NIR V-670 spectrophotometer.

RESULTS AND DISCUSSION

XRD patterns

The phase structure and crystallinity of the MCZFO-T20 and MCZFO-PE600 nanoparticles were studied using the XRD patterns, shown in Fig. 1. As can be seen, both the nanoparticles exhibit the similar XRD patterns which are consistent with offered JCPDS number (051-0383) for cubic phase of copper magnesium zinc iron oxide. Additionally, XRD patterns reveal that the (220) and (440) reflections at 2Θ = 29.9° and 62.3° are slightly sharper for the MCZFO-T20 compared to the sample synthesized in the presence of PEG 600. The observation is attributed to the flake-like crystallization, arising from the oriented growth of the crystals in a 2D platelet expansion induce by tween 20.

The average size of crystallites was determined by Scherrer equation [22], revealing the potential of PEG-600 for controlling size of the nanoparticles. So that, the MCZFO-T20 nanoparticles have the crystallites in the average size of 29.21 nm, while the crystallites for the MCZFO-PEG600 are in the size of 17.3 nm.

FESEM images

Fig. 2 shows the FESEM images for the synthesized MCZFO in the presence of tween 20 and PEG-600. Fig. 2a represents the FESEM image of MCZFO-T20, indicating the flake-like nanoparticles. As mentioned above, tween 20 inhibited the particle growth, favoring the formation of plate-like particles. In contrast, PEG-600 directed the formation of nano-spherical structures (Fig. 2b) by restricting the particle growth uniformly from

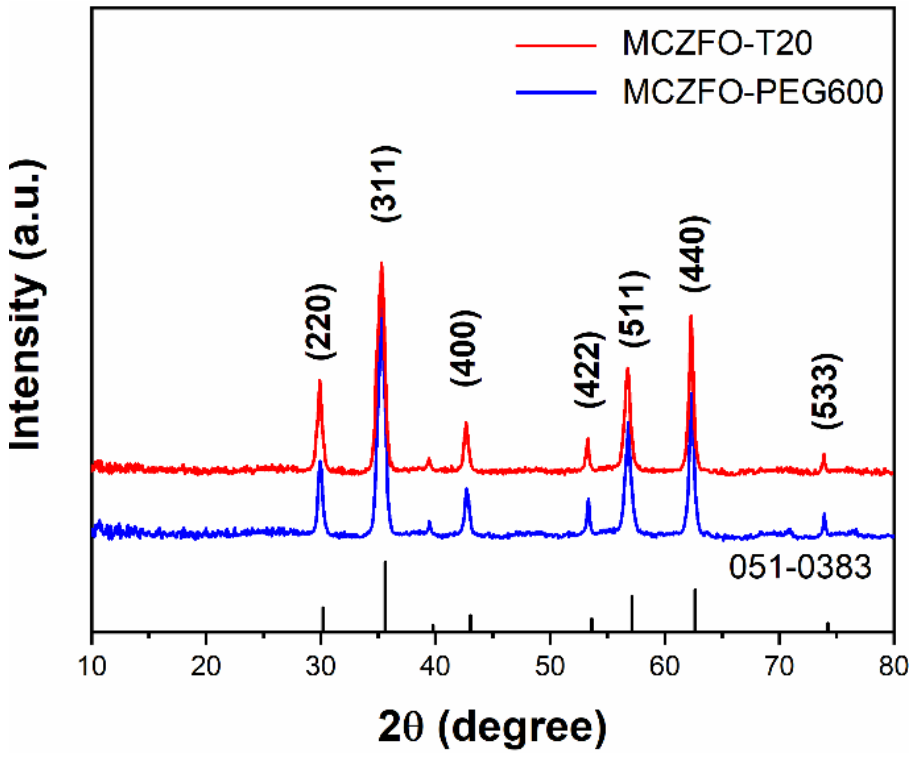

Fig. 1. XRD patterns for the synthesized MCZFO nanoparticles in the presence of tween 20 and PEG 600.

all directions. Additionally, the Fig. 2b shows the smaller size of the nanoparticles for the MCZFO-PEG600 compared to the MCZFO-T20.

The EDX spectra also provided in Fig. 2c and 2d for the MCZFO-T20 and MCZFO-PEG600, respectively. The composition of both the synthesized nanoparticles is relatively similar, as described below: MCZFO-T20: Mg (2.18%), Cu (7.92%), Zn (12.47%), Fe (47.25%), and O (30.18%); MCZFO-PEG600: Mg (1.94%), Cu (8.13%), Zn (12.75%), Fe (48.27%), and O (28.91%).

DRS analysis

UV/Vis spectra for the synthesized MCZFO-T20 and MCZFO-PEG600, shown in Fig. 3, reveal the capability of the nanoparticles serving as visible-light photocatalysts. As seen, both the nanoparticle represent prominent absorption in the range of 400 nm to 700 nm. The MCZFO-T20 nanoparticles have the higher absorption in the visible light region, which can be attributed to their larger surface area for the light harvesting resulting from the flake-like morphology. Using the Tauc method [23, 24], the optical band gaps were determined for both the MCZFO-T20 and MCZFO-PEG600. By plotting the $(\alpha h\nu)^2$ versus $h\nu$ and then extrapolating of the linear part of the curves to the horizontal axis, the band gap values were calculated to be 2.85 and 2.77 eV for the MCZFO-PEG600 and MCZFO-T20, respectively.

VSM analysis

The magnetic measurements for the synthesized nanoparticles were studied using the VSM analysis. Fig. 4 shows the M-H plots obtained at the room temperature for the MCZFO-T20 and MCZFO-PEG600. As seen from Fig. 4, both the nanoparticles exhibit the ferromagnetic behavior, which is attributed to the substitution of Cu^{2+} ions with $3d^9$ electronic

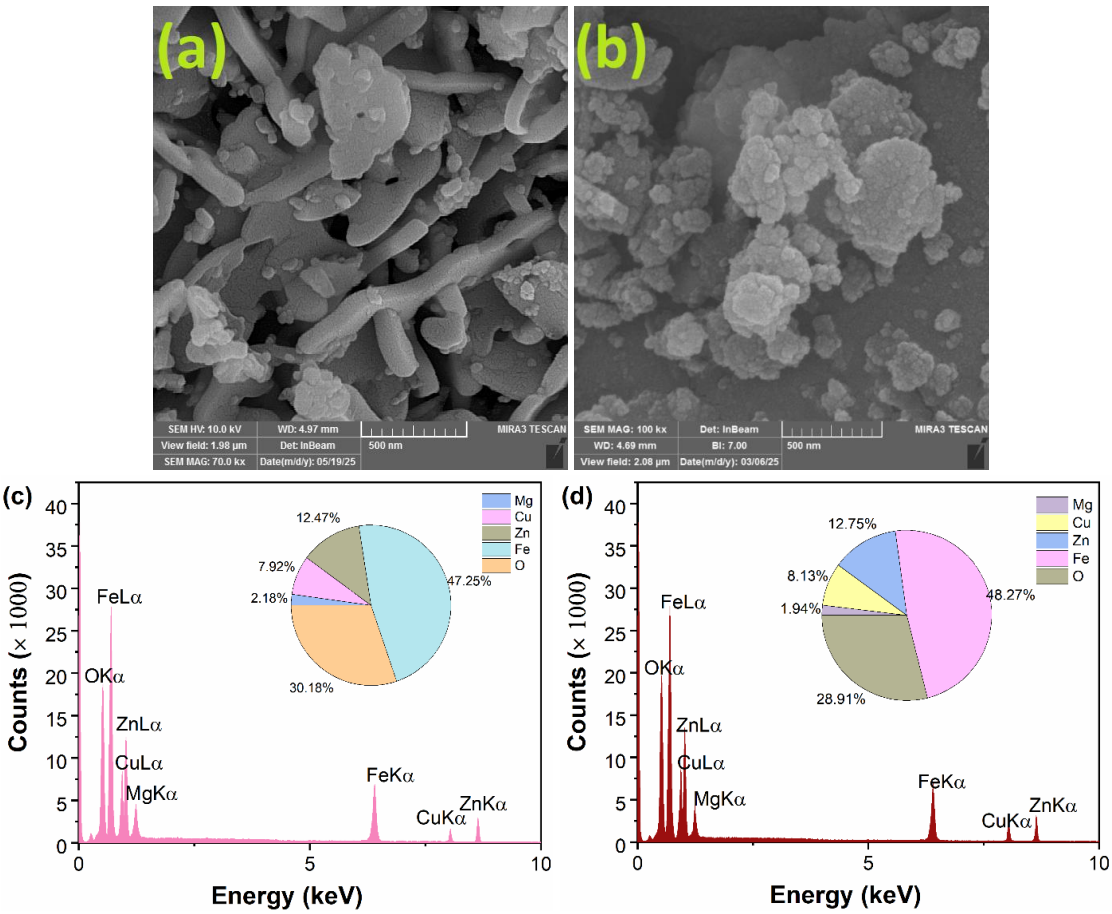

Fig. 2. FESEM images and EXD spectra for MCZFO-T20 (a, c) and MCZFO-PEG600 (b, d) nanoparticles.

configuration for the non-magnetic Zn^{2+} ions.

Additionally, the inset to the Fig. 4 shows that the flake-like MCZFO-T20 nanoparticles exhibit higher coercivity (H_c = 189.27 Oe) due to the enhanced shape anisotropy and domain wall pinning, whereas spherical nanoparticles (MCZFO-PEG600) show the reduced H_c (90.41 Oe) [25, 26]. In contrast, the spherical morphology favors easier spin alignment, resulting in the saturation magnetization (M_s = 42.96 emu/g) compared to the

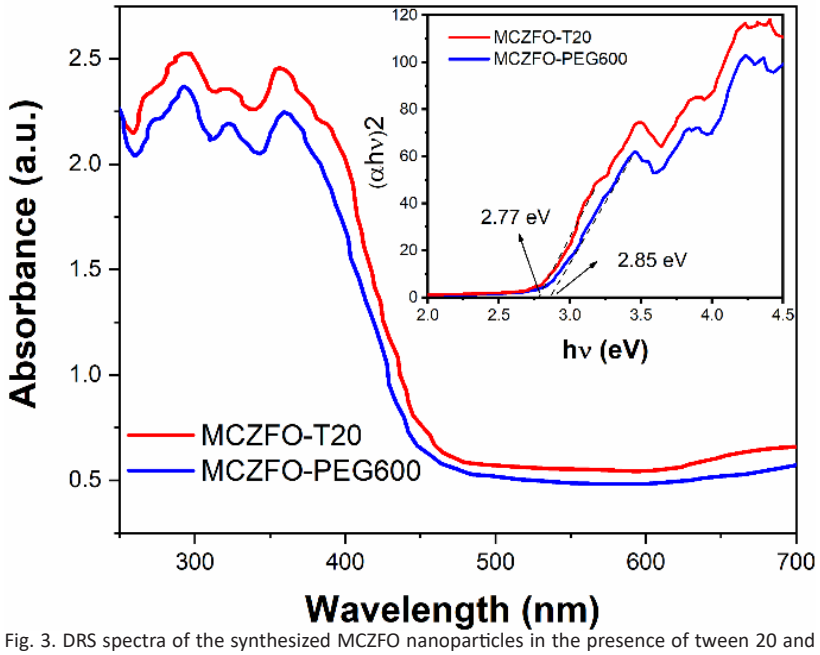

Fig. 3. DRS spectra of the synthesized MCZFO nanoparticles in the presence of tween 20 and PEG 600. The inset shows the Tauc plots.

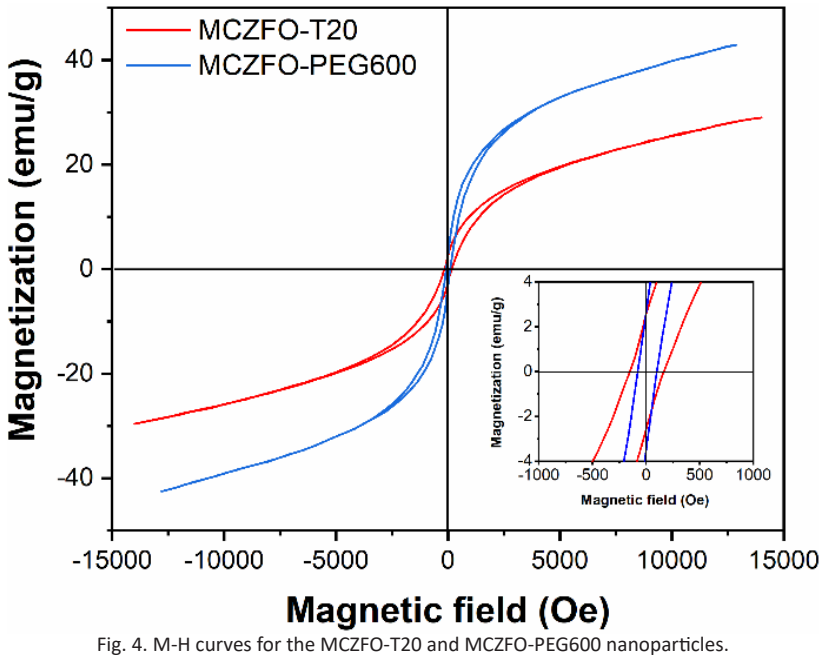

Fig. 4. M-H curves for the MCZFO-T20 and MCZFO-PEG600 nanoparticles.

lower M_s value of 29.38 emu/g for the MCZFO-T20 nanoparticles [27].

Photocatalytic experiments

Photocatalyst amount

The photocatalytic activity of the synthesized MCZFO-T20 and MCZFO-PEG600 nanoparticles was investigated for the visible-light degradation of the AR88 solution. Fig. 5 shows the AR88 was degraded by about 89% using 0.03 g of the MCZFO-T20 after 120 min illumination. Further amount of the loaded MCZFO-T20 nanoparticles led to the decrease in the degradation efficiency of the AR88. However, 0.05 g of the MCZFO-PEG600 nanoparticles were able to achieve 84% of the AR88 degradation. Similar to the results obtained by MCZFO-T20, exceeded amount of the MCZFO-PEG600 dramatically decreased the degradation level of the AR88. This observation can be justified by obstruction of the light beam penetration to the solution containing the exceeded amount of solid particles [28, 29].

Owing to the higher surface contact of the flake-like MCZFO-T20 nanoparticles, the enhanced photoactivity is achieved by lower amount of this nanoparticles compared to the MCZFO-PEG600 nanoparticles. Moreover, the self-degradation of AR88 is negligible after 120 min visible-light illumination, confirming the stability of the AR88 under no-catalyst conditions.

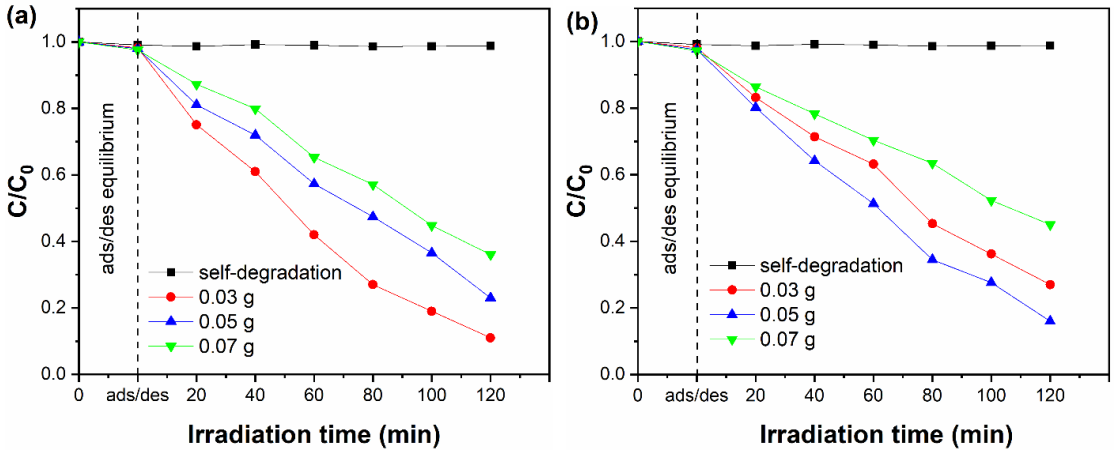

Fig. 5. Photodegradation of AR88 using different amounts of MCZFO-T20 (a) and MCZFO-PEG600 (b) nanoparticles.

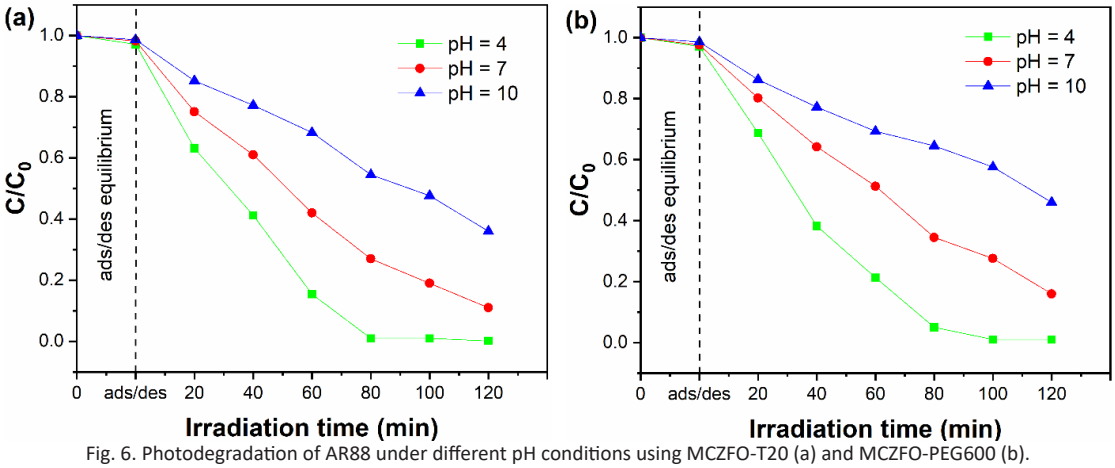

Fig. 6. Photodegradation of AR88 under different pH conditions using MCZFO-T20 (a) and MCZFO-PEG600 (b).

pH of AR88 solution

It is well known that the photocatalysis is the heterogeneous reaction which takes place between adsorbed species and generated radicals on the surface of the photocatalyst [29, 30]. Due to the anionic character of AR88, its adsorption on the positively charged surface of the catalyst is significant compared to the surface with the negative charges [31]. Therefore, it can be expected that the photocatalytic performance is increased by lowering the pH, which causes the positive charges on the surface of the photocatalyst.

Fig. 6 shows the photocatalytic efficiency of the nanoparticles under different pH values of the AR88. By adding HCl (0.2 M) until reaching pH to 3, the degradation level of AR88 approached 99% after 80 min for both of the MCZFO-T20 (0.03 g) and MCZFO-PEG600 (0.05 g) nanoparticles. However, increasing the pH by addition of NaOH (0.2 M), the photocatalytic degradation of AR88 was markedly reduced, indicating that under alkaline conditions, electrostatic repulsion hinders the adsorption of AR88 molecules onto the surface of the photocatalyst.

Oxidant agents

Fig. 7 represents the photocatalytic efficiency of the MCZFO-T20 and MCZFO-PEG600 under different amounts of $Na_2S_2O_8$ (2 mM) and H_2O_2 (2 mM) as oxidant agents. Addition of $Na_2S_2O_8$ and H_2O_2 significantly increased the photocatalytic efficiency of the AR88 solution. As can be seen form Fig. 7a, AR88 was fully degraded using 0.3 g of MCZFO-T20 nanoparticles in the presence of 1.5 mL of $Na_2S_2O_8$. Under illumination, $Na_2S_2O_8$ dissociates to sulfate radicals which then can induce formation of hydroxyl radical (•OH) according to the following reactions (Eq.1 and Eq.

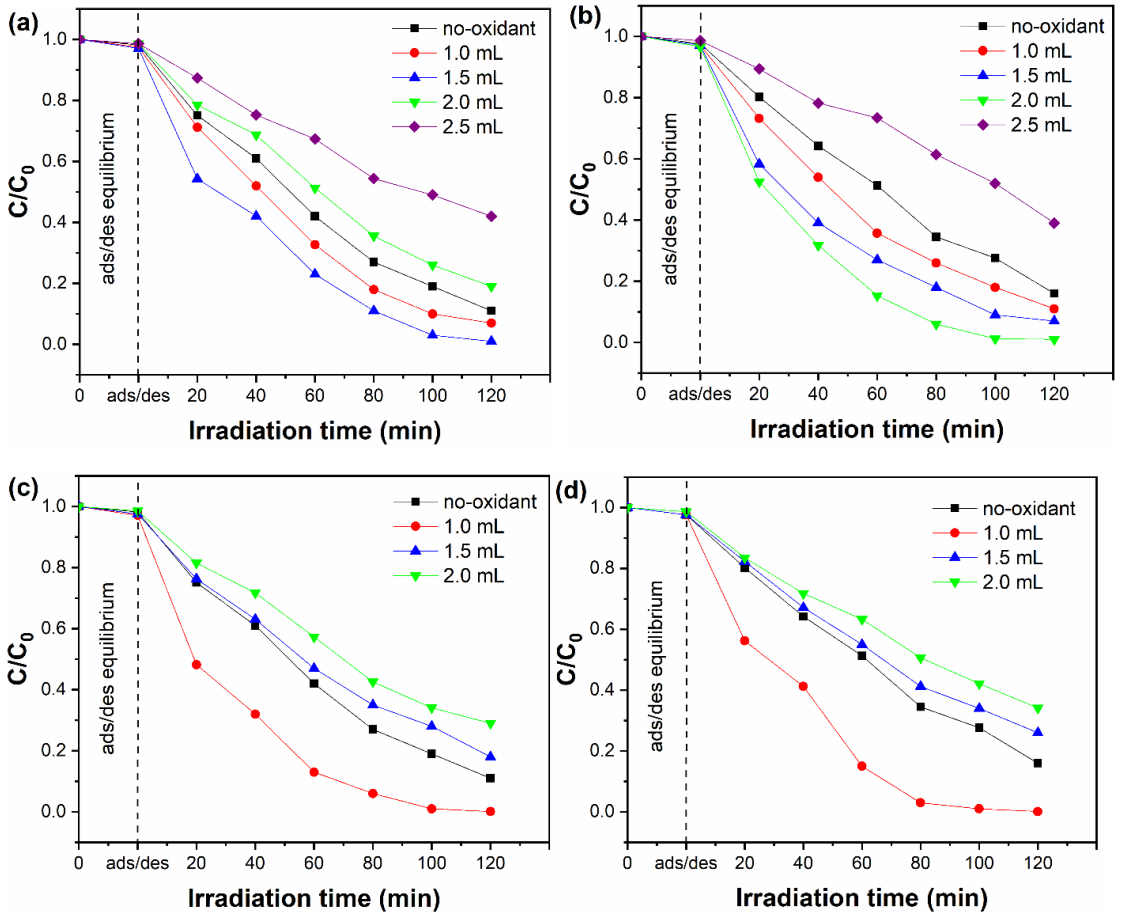

Fig. 7. Photodegradation of AR88 in the presence $Na_2S_2O_8$ and H_2O_2 using MCZFO-T20 (a, c) and MCZFO-PEG600 (b, d), respectively.

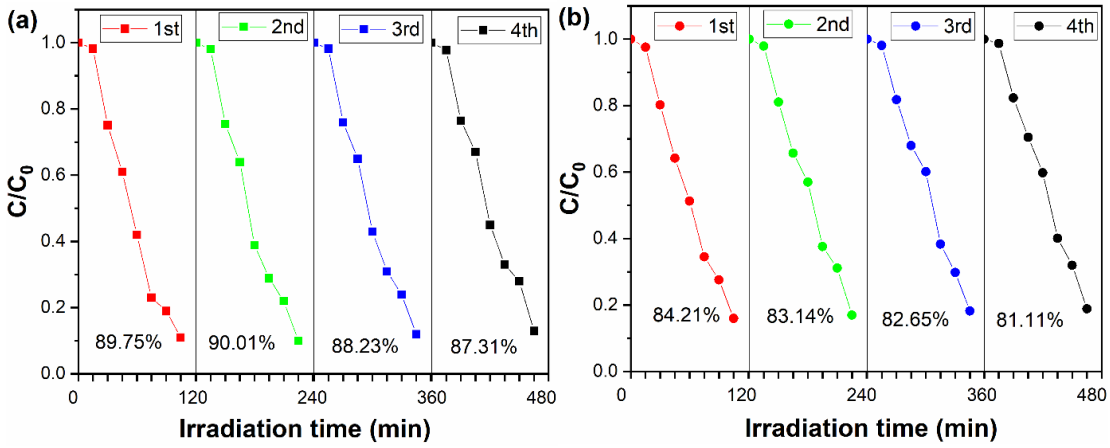

Fig. 8. Reusability experiments using MCZFO-T20 (■) and MCZFO-PEG600 (●).

2) [32, 33].

$$S_2O_8^{2-} \rightarrow 2 \bullet SO_4^-$$

$$\bullet SO_4^- + H_2O \rightarrow \bullet OH + SO_4^{2-} + H^+$$

But, exceeded amount of the $Na_2S_2O_8$ (2.0 mL) led to the significant decrement in the photocatalytic activity. This observation is attributed to the competition of $Na_2S_2O_8$ with the photocatalyst to absorb the light, thereby reducing the formation of the hydroxyl radicals using the photo-excited photocatalyst [34]. As for MCZFO-PEG600 nanoparticles (Fig. 7b), the enhanced photocatalytic degradation of AR88 was achieved by addition of 2.0 mL of the $Na_2S_2O_8$ solution.

Additionally, the effect of the H_2O_2 was investigated on the photocatalytic degradation of AR88 (Fig. 7c and 7d). H_2O_2 can effectively contribute to the formation of more radicals for the degradation of organic pollutants [35]. H_2O_2 reacts with the photo-generated electrons to form the hydroxyl radicals [35]. Fig.7c and 7d clearly show that the 1.0 mL of the H_2O_2 solution was sufficient to increase the degradation rate of both the synthesized nanoparticles. So that, after 60 min visible-light illumination, both MCZFO-T20 and MCZFO-PEG600 nanoparticles degraded the AR88 by more than 99%.

Similar to the $Na_2S_2O_8$ solution, further amount of the H_2O_2 led to the decrease in the photocatalytic degradation of the AR88. This result is assigned to the involvement of the H_2O_2 in the reactions (Eq. 3 and Eq. 4) ends up to the formation of H_2O, by consuming the hydroxyl radicals [18, 32].

$$H_2O_2 + \bullet OH \rightarrow H_2O + \bullet H_2O$$

$$\bullet H_2O + \bullet OH \rightarrow H_2O + O_2$$

Reusability experiments

The reusability is the important properties for the practical photocatalyst materials [36]. Fig. 8 shows the 4-cycle reusability experiments conducted for both the MCZFO-T20 and MCZFO-PEG600 nanoparticles. After each reaction cycles, the nanoparticles were separated, washed several times with distilled water, and then dried in an oven at 90 °C for 3 h. Fig. 8 a and b disclose that the synthesized MCZFO-T20 and MCZFO-PEG600 nanoparticles have the great stability to degrade the AR88 over 4 consecutive reaction cycles. The decrease in the photocatalytic efficiency was about 2.44% and 3.12% for the MCZFO-T20 and MCZFO-PEG600 nanoparticles, respectively.

CONCLUSION

This work reported the synthesis of $Mg_{0.2}Cu_{0.3}Zn_{0.5}Fe_2O_4$ (MCZFO) nanoparticles using co-precipitation method in the presence of different capping agents, including tween 20 and PEG 600. The MCZFO nanoparticles synthesized by tween 20 (MCZFO-T20) exhibited flake-like morphology which caused the enhanced optical, magnetic, and photocatalytic properties compared to the

spherical nanoparticles synthesized using PEG 600 (MCZFO-PEG600). The optical investigations of the synthesized nanoparticles showed the MCZFO-T20 have the improved light absorption in the visible light region. In addition, the calculated band gaps for the nanoparticles revealed the MCZFO-T20 nanoparticles have the narrower band gap (2.77 eV compared to 2.85 eV for the MCZFO-PEG600), which is attributed to their nano-flake morphology allowing the stronger interaction with the incident light beams.

The magnetic measurements revealed the ferromagnetic behavior for both the nanoparticles. Due to the shape anisotropy of the flake-like nanoparticles, the coercivity value for the MCZFO-T20 nanoparticles is higher than MCZFO-PEG600. However, the MCZFO-PEG600 showed the higher magnetization saturation, attributed to the easier spin alignment resulting from the isotropic nature of the spherical nanoparticles.

The photocatalytic activity of the nanoparticles was tested by the visible-light degradation of AR88, showing the enhanced photoactivity for the MCZFO-T20 nanoparticles. More than 89% of the AR88 solution was degraded using MCZFO-T20 nanoparticles after 120 min illumination under visible light irradiation. At the same time irradiation, the MCZFO-PEG600 showed the photocatalytic efficiency of 84%. The photocatalytic performance was studied under varied experimental conditions, which revealed the higher photoactivity under acidic conditions and optimum concentrations of H_2O_2 and $Na_2S_2O_8$ solutions. Also, the synthesized nanoparticles exhibited the great reusability over 4 successive reaction cycles.

CONFLICT OF INTEREST

The authors declare that there is no conflict of interests regarding the publication of this manuscript.

REFERENCES

1. Joudeh N, Linke D. Nanoparticle classification, physicochemical properties, characterization, and applications: a comprehensive review for biologists. Journal of Nanobiotechnology. 2022;20(1).
2. Altammar KA. A review on nanoparticles: characteristics, synthesis, applications, and challenges. Front Microbiol. 2023;14.
3. Christian P, Von der Kammer F, Baalousha M, Hofmann T. Nanoparticles: structure, properties, preparation and behaviour in environmental media. Ecotoxicology. 2008;17(5):326-343.
4. Anu Mary Ealia S, Saravanakumar MP. A review on the classification, characterisation, synthesis of nanoparticles and their application. IOP Conference Series: Materials Science and Engineering. 2017;263:032019.
5. Cuenya BR. Synthesis and catalytic properties of metal nanoparticles: Size, shape, support, composition, and oxidation state effects. Thin Solid Films. 2010;518(12):3127-3150.
6. Lin X-M, Samia ACS. Synthesis, assembly and physical properties of magnetic nanoparticles. J Magn Magn Mater. 2006;305(1):100-109.
7. Brenner S. Nanomedicine: promises and challenges for the future of public health. International Journal of Nanomedicine. 2010:803.
8. Patil SS, Shedbalkar UU, Truskewycz A, Chopade BA, Ball AS. Nanoparticles for environmental clean-up: A review of potential risks and emerging solutions. Environmental Technology and Innovation. 2016;5:10-21.
9. Santos CSC, Gabriel B, Blanchy M, Menes O, García D, Blanco M, et al. Industrial Applications of Nanoparticles – A Prospective Overview. Materials Today: Proceedings. 2015;2(1):456-465.
10. Chen Y, Agrelo-Lestón A, Burgués-Ceballos I, Llorca J, Soler L. Bimetallic Nanoparticles as Cocatalysts for Photocatalytic Hydrogen Production. Adv Funct Mater. 2025.
11. Hajjaji MA, Missaoui K, Trabelsi K, Bouzaza A, Hajjaji A, Bessais B, et al. Platinum nanoparticles decorated TiO_2 nanotubes for VOCs and bacteria removal in simulated real condition: Effect of the deposition method on the photocatalytic degradation process efficiency. J Photochem Photobiol A: Chem. 2025;458:115975.
12. Ashraf GA, Al-Sulaimi S, Hassan N, Ajmal Z, Mahmood S, Rasool RT, et al. Mesoporous Carbon@ZnCuFeS nanoparticles for photocatalytic degradation of organic pollutants via peroxymonosulfate activation. J Organomet Chem. 2025;1032:123624.
13. Schneider J, Matsuoka M, Takeuchi M, Zhang J, Horiuchi Y, Anpo M, et al. Understanding TiO_2 Photocatalysis: Mechanisms and Materials. Chem Rev. 2014;114(19):9919-9986.
14. Pelaez M, Nolan NT, Pillai SC, Seery MK, Falaras P, Kontos AG, et al. A review on the visible light active titanium dioxide photocatalysts for environmental applications. Applied Catalysis B: Environmental. 2012;125:331-349.
15. Iervolino G, Zammit I, Vaiano V, Rizzo L. Limitations and Prospects for Wastewater Treatment by UV and Visible-Light-Active Heterogeneous Photocatalysis: A Critical Review. Topics in Current Chemistry Collections: Springer International Publishing; 2019. p. 225-264.
16. Peiris S, de Silva HB, Ranasinghe KN, Bandara SV, Perera IR. Recent development and future prospects of TiO_2 photocatalysis. J Chin Chem Soc. 2021;68(5):738-769.
17. Humayun M, Raziq F, Khan A, Luo W. Modification strategies of TiO_2 for potential applications in photocatalysis: a critical review. Green Chemistry Letters and Reviews. 2018;11(2):86-102.
18. Rahbar M, Hosseini-Sarvari M. Natural sunlight-driven photocatalytic mineralization of petrochemical wastewater using ceramic-supported Fe, B co-doped TiO_2/CNT@WO_3 in a flat panel photoreactor. Journal of Water Process Engineering. 2025;77:108328.
19. You C, Zhang X, Zhao Y, Yan R, Shen Y, Xue Q, et al. Plasmonic effect augmented S-scheme mechanism in Ag/Ag_2O/C_3N_5 photocatalyst enables efficient photocatalytic degradation of antibiotics. Journal of Materials Science and Technology. 2026;242:64-74.
20. Ai Y, Carabineiro SAC, Xiong X, Zhu H, Wang Q, Weng B,

et al. Systematic assessment of emerging contaminants elimination using an S-scheme $Mn_{0.5}Cd_{0.5}S/In_2S_3$ photocatalyst: Degradation pathways, toxicity evaluation and mechanistic analysis. Chinese Journal of Catalysis. 2025;75:147-163.
21. Sulaiman NH, Ghazali MJ, Yunas J, Rajabi A, Majlis BY, Razali M. Synthesis and characterization of $CaFe_2O_4$ nanoparticles via co-precipitation and auto-combustion methods. Ceram Int. 2018;44(1):46-50.
22. Holder CF, Schaak RE. Tutorial on Powder X-ray Diffraction for Characterizing Nanoscale Materials. ACS Nano. 2019;13(7):7359-7365.
23. Abed SH, Shamkhi AF, Heydaryan K, Mohammadalizadeh M, Sajadi SM. Sol-gel Pechini preparation of $CuEr_2TiO_6$ nanoparticles as highly efficient photocatalyst for visible light degradation of acid red 88. Ceram Int. 2024;50(13):24096-24102.
24. Jubu PR, Obaseki OS, Ajayi DI, Danladi E, Chahrour KM, Muhammad A, et al. Considerations about the determination of optical bandgap from diffuse reflectance spectroscopy using the tauc plot. Journal of Optics. 2024;53(5):5054-5064.
25. Mohapatra J, Fischbacher J, Gusenbauer M, Xing MY, Elkins J, Schrefl T, et al. Coercivity limits in nanoscale ferromagnets. Physical Review B. 2022;105(21).
26. Tadic M, Kopanja L, Panjan M, Lazovic J, Tadic BV, Stanojevic B, et al. Rhombohedron and plate-like hematite (α-Fe_2O_3) nanoparticles: synthesis, structure, morphology, magnetic properties and potential biomedical applications for MRI. Mater Res Bull. 2021;133:111055.
27. Issa B, Obaidat I, Albiss B, Haik Y. Magnetic Nanoparticles: Surface Effects and Properties Related to Biomedicine Applications. Int J Mol Sci. 2013;14(11):21266-21305.
28. Anandan S, Sathish Kumar P, Pugazhenthiran N, Madhavan J, Maruthamuthu P. Effect of loaded silver nanoparticles on TiO_2 for photocatalytic degradation of Acid Red 88. Sol Energy Mater Sol Cells. 2008;92(8):929-937.
29. Rahbar M, Mehrzad M, Behpour M, Mohammadi-Aghdam S, Ashrafi M. S, N co-doped carbon quantum dots/TiO_2 nanocomposite as highly efficient visible light photocatalyst. Nanotechnology. 2019;30(50):505702.
30. Van Doorslaer X, Demeestere K, Heynderickx PM, Van Langenhove H, Dewulf J. UV-A and UV-C induced photolytic and photocatalytic degradation of aqueous ciprofloxacin and moxifloxacin: Reaction kinetics and role of adsorption. Applied Catalysis B: Environmental. 2011;101(3-4):540-547.
31. Daneshvar N, Salari D, Khataee AR. Photocatalytic degradation of azo dye acid red 14 in water on ZnO as an alternative catalyst to TiO_2. J Photochem Photobiol A: Chem. 2004;162(2-3):317-322.
32. Wang Y, Hong C-s. Effect of hydrogen peroxide, periodate and persulfate on photocatalysis of 2-chlorobiphenyl in aqueous TiO_2 suspensions. Water Res. 1999;33(9):2031-2036.
33. Kolthoff IM, Miller IK. The Chemistry of Persulfate. I. The Kinetics and Mechanism of the Decomposition of the Persulfate Ion in Aqueous Medium 1. Journal of the American Chemical Society. 1951;73(7):3055-3059.
34. Saadati A, Habibi-Yangjeh A, Khataee A. Activation of persulfate ions by QDs-sized Z-scheme $TiO_{2-x}/Cu_3Mo_2O_9$ photocatalysts in visible-light detoxification of organic contaminants. J Alloys Compd. 2023;969:172322.
35. Gaya UI, Abdullah AH. Heterogeneous photocatalytic degradation of organic contaminants over titanium dioxide: A review of fundamentals, progress and problems. Journal of Photochemistry and Photobiology C: Photochemistry Reviews. 2008;9(1):1-12.
36. Shirazi P, Rahbar M, Behpour M, Ashrafi M. La_2MnTiO_6 double perovskite nanostructures as highly efficient visible light photocatalysts. New J Chem. 2020;44(1):231-238.